Lys05 – A Promising Autophagy Inhibitor in the Radiosensitization Battle: Phosphoproteomic Perspective

MARTIN ONDREJ[1], LUCIE CECHAKOVA[1], IVO FABRIK[2], JANA KLIMENTOVA[2] and ALES TICHY[1]

[1]Department of Radiobiology, Faculty of Military Health Sciences,
University of Defense in Brno, Hradec Kralove, Czech Republic;
[2]Department of Molecular Biology and Pathology, Faculty of Military
Health Sciences, University of Defense in Brno, Hradec Kralove, Czech Republic

Abstract. *Background: Autophagy is a crucial factor contributing to radioresistance during radiotherapy. Although Lys05 has proven its ability to improve the results of radiotherapy through the inhibition of autophagy, molecular mechanisms of this inhibition remain elusive. We aimed to describe the molecular mechanisms involved in Lys05-induced inhibition of autophagy. Materials and Methods: Radioresistant human non-small cell lung carcinoma cells (H1299, p53-negative) and methods of quantitative phosphoproteomics were employed to define the molecular mechanisms involved in Lys05-induced inhibition of autophagy. Results: We confirmed that at an early stage after irradiation, autophagy was induced, whereas at a later stage after irradiation, it was inhibited. The early-stage induction of autophagy was characterized mainly by the activation of biosynthetic and metabolic processes through up- or down-regulation of the critical autophagic regulatory proteins Sequestosome-1 (SQSTM1) and proline-rich AKT1 substrate 1 (AKT1S1). The late-stage inhibition of autophagy was attributed mainly to down-regulation of Unc-51 like autophagy-activating kinase 1 (ULK1) through phosphorylation at Ser638. Conclusion: This work contributes to emerging phosphoproteomic insights into autophagy-mediated global signaling in lung cancer cells, which might consequently facilitate the development of precision medicine therapeutics.*

This article is freely accessible online.

Correspondence to: Associate Professor Ales Tichy, PharmD, Ph.D., Faculty of Military Health Sciences, University of Defense in Brno, Trebesska 1575, 500 01, Hradec Kralove, Czech Republic. E-mail: ales.tichy@unob.cz

Lung cancer is one of the most widespread tumor diseases worldwide. Approximately 80% of all lung cancer cases are non-small cell lung cancer (NSCLC) (1, 2). Treatment of NSCLC includes several approaches from which radiation therapy (RT) is one of the most common. According to radiation oncologists, radioresistance seems to be the most severe issue in treatment efficacy, and importantly, it involves autophagy as a crucial factor (3).

Autophagy is a natural degradation mechanism allowing the regulated destruction and recycling of cellular components in order to maintain homeostasis, especially during stress conditions (4). This degradation process takes place in both healthy and cancer cells. Figure 1 briefly depicts the critical steps of the autophagic process. The leading role of autophagy in emerging tumors is to provide nutrients and other metabolic precursors and thus maintain survival. On the other hand, developed tumors do not usually suffer from a nutrient shortage. However, they are often exposed to various kinds of anticancer therapy, which causes an extensive amount of cellular stress. Under these conditions, autophagy takes part in the elimination of toxic species (*e.g.* free radicals, damaged and misfolded proteins or organelles) and plays a cytoprotective role (5). Therefore, inhibition of autophagy seems to be a practical approach for improving cancer therapy.

Several studies have already described the sensitizing effects of autophagy inhibitors against ionizing radiation (IR) (5). For example, both Chen *et al.* (6) and Tao *et al.* (7) referred to the radiosensitization of esophageal squamous cell carcinoma using 3-methyladenine as an autophagy inhibitor. Similarly, Park *et al.* observed the radiosensitization of colorectal cancer cells due to the accumulation of DNA damage using spautin-1 as an autophagy inhibitor (8).

In our recent study, we described the effect of autophagy inhibitor Lys05 together with IR, which reduced the survival of H1299 NSCLC cells compared to the inhibitor or IR alone (9). Lys05 is a relatively new inhibitor that was firstly introduced by McAfee *et al.* (10). Chemically, it is a dimeric
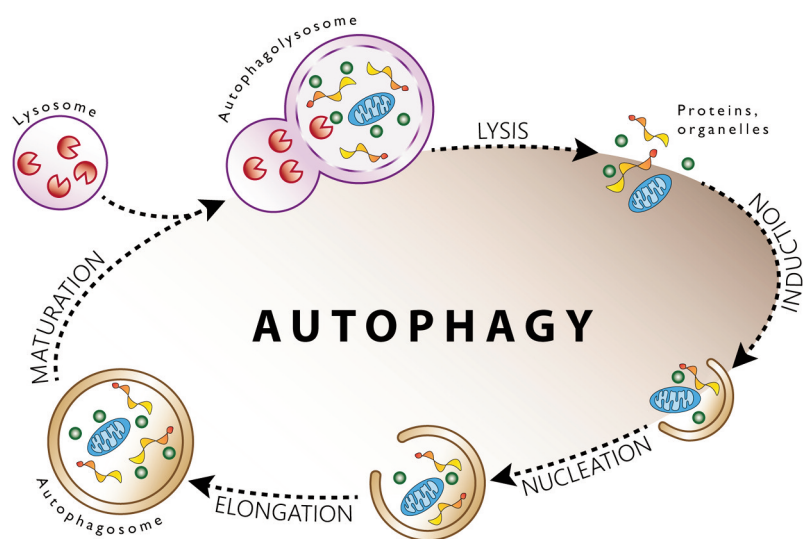
Figure 1. *Schematic overview of the autophagic process. Various stimuli such as starvation, oxygen shortage, and ionizing radiation induce autophagy. Initially, a phagophore is formed and begins to encapsulate molecules that will degrade. Subsequent nucleation and elongation lead to the formation of the characteristic double-membraned autophagosome. After the formation of the autophagosome, lysosome approaches to fuse. The formation of an autophagolysosome accompanies fusion. After fusion, the degradation of the sequestered cytoplasmic cargo involves several acid hydrolases. These hydrolases are then recycled.*

form of chloroquine which accumulates within lysosomes and thus inhibits autophagosome–lysosome fusion (10). We examined the effects of Lys05 on H1299 cells, mostly using classical biological methods. However, a deeper understanding of the molecular mechanisms underlying Lys05-mediated radiosensitization is still required.

The present study aimed to investigate the mechanisms of radiosensitization of H1299 NSCLC cells. As in our previous work, we applied Lys05 as the autophagy inhibitor, and using the methods of quantitative phosphoproteomics, we studied the mechanisms of autophagy inhibition and subsequent radiosensitization.

Materials and Methods

Cells and cultivation. H1299 Non-small cell lung carcinoma cells were obtained from the American Type Culture Collection (Manassas, VA, USA). Cells were cultured at 37˚C in a humidified incubator under 5% CO_2 and maintained in RPMI medium 1640 (Gibco, Paisley, UK) supplemented with a 10% fetal bovine serum, 150 Ul/ml penicillin and 50 mg/ml streptomycin (all from Sigma-Aldrich, St. Louis, MO, USA). The maintenance culture was divided twice per week by dilution to a density of 2×10^5 cells/10 ml. The cell line was used up to a maximum of 15 passages for this study.

Stable isotope labeling by amino acids in cell culture (SILAC). The phosphoproteomic analysis was performed using a SILAC-based approach, as described previously (11). For labeling, H1299 cells were divided into two groups and transferred into SILAC RPMI

medium (Gibco) with the addition of either non-labeled L-lysine (32 mg/l), L-arginine (200 mg/l) and L-glutamine (300 mg/l) – a 'light' group or labeled L-lysine-4,4,5,5-d_4 hydrochloride,L-arginine-$^{13}C_6$ hydrochloride and L-glutamine (in equimolar amounts) – a 'heavy' group, both supplemented with 10% dialyzed fetal bovine serum, 150 Ul/ml penicillin and 50 mg/ml streptomycin (all from Sigma-Aldrich). L-Proline (300 mg/l) was added to the media to avoid the metabolic conversion of arginine to proline (12). At least six doublings were required for the full incorporation of labeled amino acids.

Cell treatment. The cells from the heavy group were treated by autophagy inhibitor Lys05 (a kind gift of Dr. Ravi Amaravadi, Pennsylvania University, Philadelphia, PA, USA) at a concentration of 2 μM. The inhibitor was added to the cells 1 h before irradiation. The cells from the light group were left untreated. Both groups were irradiated with a single dose of 2 Gy using a ^{60}Co gamma-ray source at a dose rate of 1.04 Gy/min. After irradiation, each group was divided into two subgroups, returned to an incubator and cultivated further for a 1 and 48 h, respectively.

Recovery of proteins. The cells were lysed using a lysis buffer with the composition of 50 mM ammonium bicarbonate, 1% sodium deoxycholate, and phosphatase inhibitor cocktails 2 and 3 (Sigma-Aldrich). The appropriate subgroups of 'heavy' and 'light' proteins were pooled together in a 1:1 ratio and digested with trypsin (Sequencing Grade Modified Trypsin; Promega Corporation, Madison, WI, USA) as mentioned elsewhere (11). Thus, two sets of cells were formed: Set 1 consisting of light and heavy cells processed 1 h after irradiation and Set 2 consisting of light and heavy cells processed 48 h after irradiation. Figure 2 schematically depicts the procedure of our experiment.
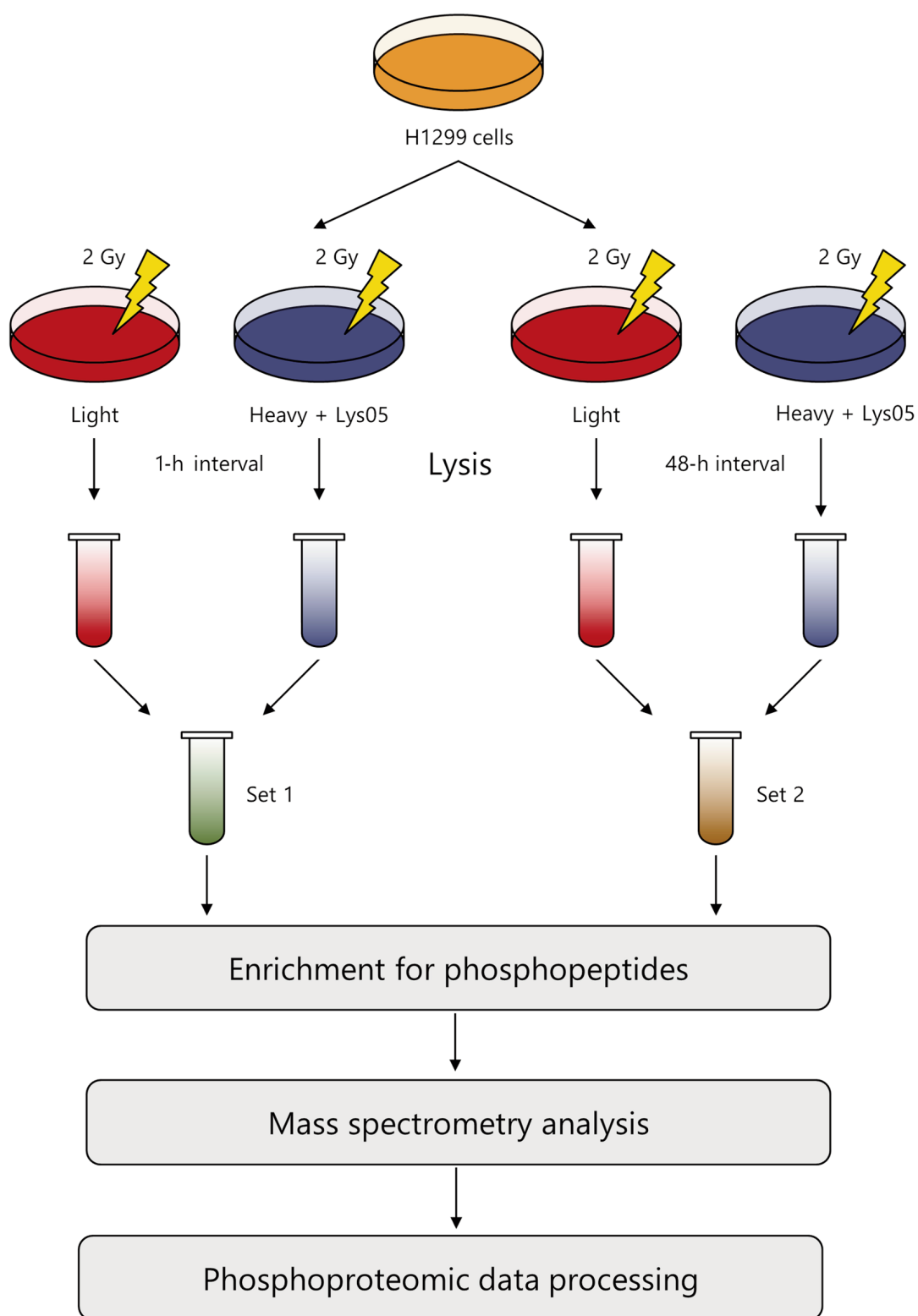
Figure 2. *The workflow of sample processing. H1299 cells were irradiated and cultivated in a 'heavy' or 'light' stable isotope labeling by amino acids in cell culture (SILAC) medium. One and 48 h after irradiation, the cells were lysed and samples from the heavy and light media were pooled together to form Set 1 and Set 2, respectively. Samples from both sets were enriched for phosphopeptides, analyzed using mass spectrometry and processed based on the principles of quantitative phosphoproteomics.*
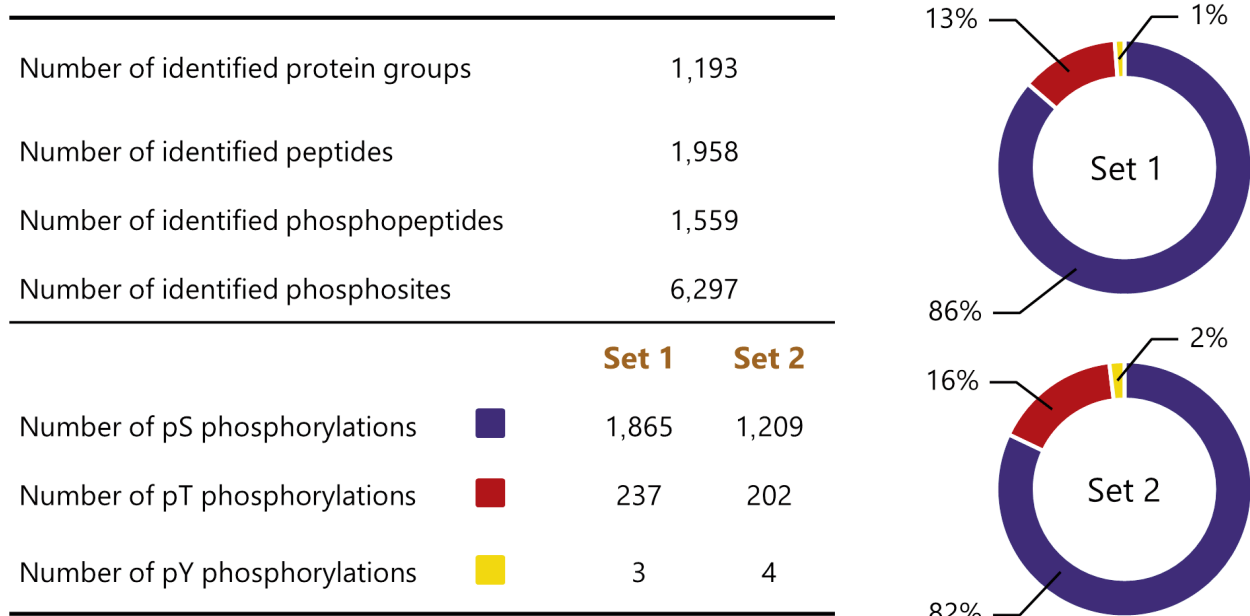
			Set 1	Set 2
Number of identified protein groups		1,193		
Number of identified peptides		1,958		
Number of identified phosphopeptides		1,559		
Number of identified phosphosites		6,297		
Number of pS phosphorylations			1,865	1,209
Number of pT phosphorylations			237	202
Number of pY phosphorylations			3	4

Figure 3. *A general overview of the phosphoproteomic analysis. The table indicates the number of identified proteins, peptides, phosphopeptides, and phosphosites. The number of phosphorylations refers to identified phosphorylations of a particular amino acid in each set: pS: serine, pT: threonine, pY: tyrosine. The percentage distribution of phosphorylation among serine (blue), threonine (red), and tyrosine (yellow) residues is visualized using the ring plots.*

Enrichment for phosphopeptides. After digestion, redundant sodium deoxycholate was extracted by ethyl acetate (13) and samples from both sets were desalted using C18 solid-phase extraction cartridges (3M™ Empore™, St. Paul, MN, USA) with subsequent elution by 60% acetonitrile/0.1% trifluoroacetic acid. Afterward, the samples were enriched for phosphopeptides using titanium dioxide chromatography (14). Enrichment for phosphopeptides was performed using Mobicol spin columns (MoBiTec GmbH, Goettingen, Germany). Firstly, the samples were supplemented with loading buffer (65% acetonitrile, 2% TFA, 100 mM glutamic acid). Then titanium dioxide microparticles (Titansphere® 5 μm particles; GL Sciences, Torrance, CA, USA) suspended in loading buffer were added to the samples (peptide:TiO_2 ratio, 1:10) and left mixing for 30 minutes at room temperature. Afterward, the microparticles were washed with 200 μl of loading buffer, 200 μl of washing buffer 1 (65% acetonitrile with 0.5% TFA), then sequentially with 200 μl and 100 μl of washing buffer 2 (65% acetonitrile with 0.1% TFA). Phosphopeptides were then eluted by 150 μl of elution buffer (NH_4OH, pH 11.5). After elution, they were acidified with 10% TFA to pH 2 and desalted using C18 spin columns (Harvard Apparatus, Holliston, MA, USA). Desalted TiO_2-enriched peptides were dried out in an Eppendorf™ Concentrator Plus (Eppendorf, Hamburg, Germany).

Mass spectrometry. For the mass spectrometric analysis, we used a Dionex Ultimate™ 3000 RSLCnano system coupled through Nanospray Flex ion source with a Q-Exactive mass spectrometer (both Thermo Fisher Scientific, Bremen, Germany). The TiO_2-enriched peptide mixture (2% acetonitrile/0.05% TFA; 1 μl) was injected onto a capillary trap column (C18 PepMap100, 3 μm, 100 A, 0.075×20 mm; Dionex) and then eluted and separated on capillary column (C18 PepMap RSLC, 2 μm, 100 A, 0.075×150 mm; Dionex) with a step linear gradient of mobile phase B (80% acetonitrile/0.1% formic acid) over mobile phase A (0.1% formic acid) from 4% to 34% B in 68 minutes and from 34% to 55% B in 21 minutes, at flow rate of 300 nl/min. The column was maintained at 40˚C and the eluent was monitored at 215 nm.

Phosphoproteomic data processing. Raw mass spectrometric files were processed with MaxQuant software v. 1.5.6.5 (available online: https://maxquant.org) (15). Peak lists were searched against the human UniProt database using the Andromeda search engine (16). The parameters applied for protein identification were: MS/MS tolerance=0.02 Da; peptide mass tolerance for MS=6 ppm and for MS2=20 ppm; missed cleavages=0; enzyme=trypsin; fixed modification: carbamidomethyl (C) and variable modification: oxidation (M), acetyl (protein N-term), phospho (STY). Additionally, appropriate SILAC labels were selected (Arg6, Lys4). Only proteins, peptides, and phosphorylation sites with a false-discovery rate (FDR) lower than 0.01 were accepted. Both razor and unique peptides were used for the calculation of heavy/light protein ratios.

Statistical analysis. Statistical analysis was performed using Perseus software v. 1.5.6.0 (available online: https://maxquant.net/perseus). Contaminants and reversed hits were removed first before further data processing. To identify significantly differentially regulated phosphosites, 'Significance B test' was used with Benjamini-Hochberg FDR correction (FDR<0.05). Proteins with differentially regulated phosphosites were subjected to Gene Ontology (GO) analysis. GO analysis was performed using the ConsensusPathDB
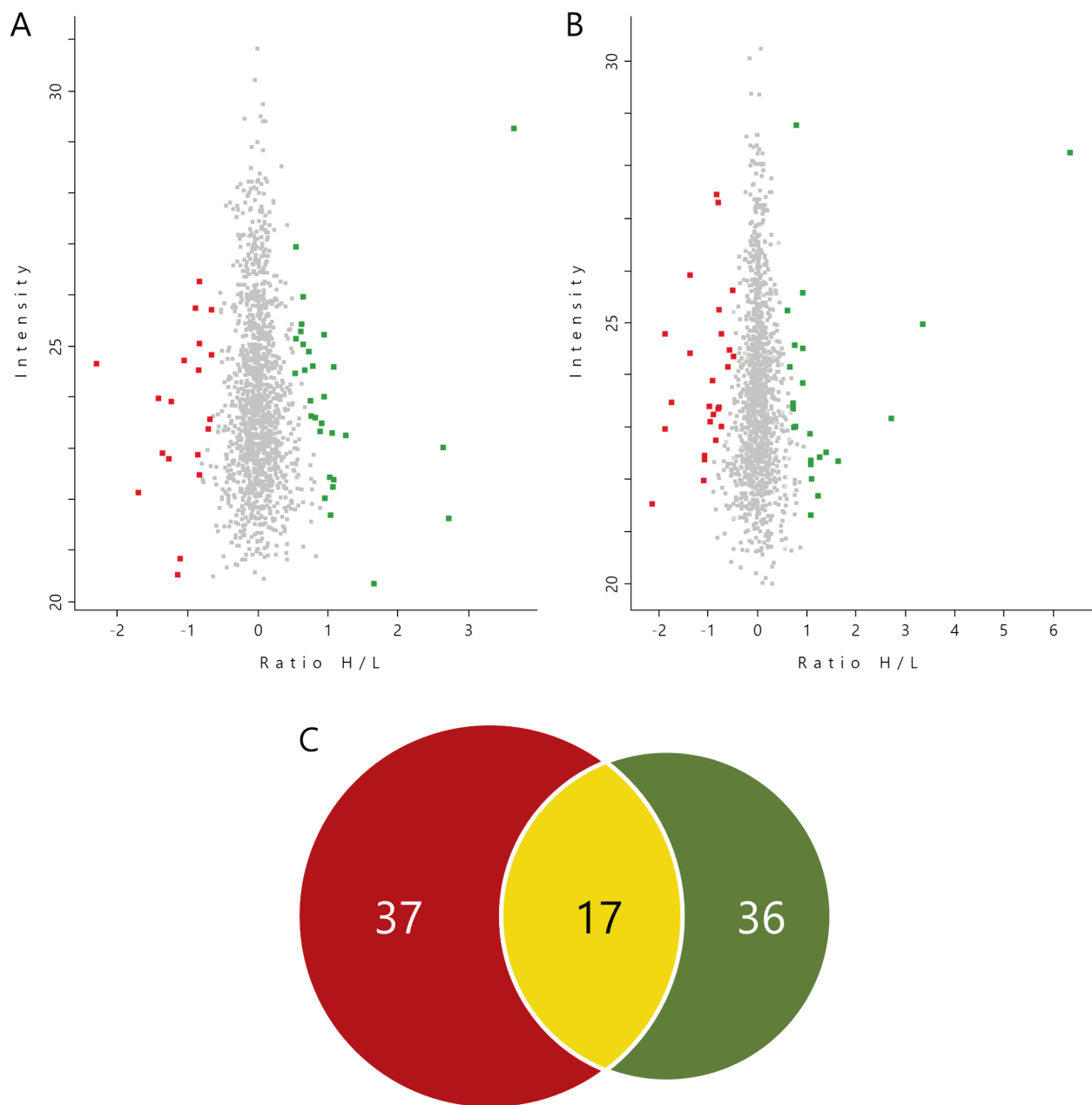
Figure 4. *Overview of proteins with differentially regulated phosphosites. A: Proteins with significantly differentially regulated phosphosites identified 1 h after irradiation (Set 1). B: Proteins with significantly differentially regulated phosphosites identified 48 h after irradiation (Set 2). C: Venn diagram of proteins with differentially regulated phosphosites identified 1 h (red) and 48 h (green) after irradiation. H: Heavy labeled; L: light labeled.*

over-representation analysis web tool v. 32 (*p*-value<0.01; available online: http://consensuspathdb.org). We deployed STRING software v. 10.5 (available online: http://string-db.org) to identify potential protein-protein interactions of phosphorylated proteins, applying a minimum confidence score of 0.4 and a maximum number of 20 additional interactors (added by the STRING software). The resulting inferred networks were visualized using the STRING network viewer.

Results

General phosphoproteomic description. We performed a phosphoproteomic (SILAC-based) analysis to investigate the mechanisms involved in the radiosensitization of H1299 cells mediated by the abrogation of autophagy. In general, we worked with two sets of H1299 cells: i) Those processed 1

h after irradiation (Set 1), and ii) those processed 48 h after irradiation (Set 2).

Overall, we identified 1,193 protein groups with 6,297 phosphorylation sites (Figure 3). Of these proteins, the most abundantly phosphorylated amino acid detected in both Set 1 and Set 2 was serine (86% and 82%, respectively), followed by threonine (13% and 16%, respectively) and tyrosine (1% and 2%, respectively) (Figure 3).

Overview of the differentially regulated phosphosites. Differential regulation of phosphosites correlated with an impact of the inhibitor on H1299 cells and with subsequent changes in the signaling pathways. We identified 54 proteins with differentially regulated phosphosites in Set 1. In this Set, we observed the up-regulation of 33 phosphosites and down-regulation of 21 phosphosites (Figure 4A). Additionally, we identified 53 proteins with differentially regulated phosphosites in Set 2. This Set included 26 up-regulated and 27 down-regulated phosphosites (Figure 4B). Finally, we detected 17 phosphosites differentially regulated in both sets (Figure 4C). Tables I and II summarize all proteins with differentially regulated phosphosites identified in sets 1 and 2, respectively.

GO analysis suggests delayed onset of autophagy inhibition in H1299 cells. In order to biologically evaluate proteins with differentially regulated phosphosites, we subjected both sets to GO analysis. According to the ConsensusPathDB GO analysis (level 4 terms), most of the proteins with differentially regulated phosphosites from Set 1 (displayed in Figure 5A) were localized in various parts of the nucleus. On the other hand, proteins with differentially regulated phosphosites from Set 2 (displayed in Figure 5B) were localized in both the nucleus and the cytosol. Proteins with differentially regulated phosphosites found in both sets performed molecular functions associated with transcription and RNA binding.

In terms of biological processes, proteins with differentially up-regulated phosphosites from Set 1 took part mostly in cellular transport, biosynthetic and metabolic processes, gene expression, and in response to heat. The up-regulation of biosynthetic, metabolic, and transporting processes might represent one of the specific signs indicating activation of autophagy. Moreover, up-regulated processes of response to heat might be associated with the cellular reaction to various kinds of stress. On the other hand, proteins with differentially down-regulated phosphosites from Set 1 took part in processes associated with the regulation of cell growth (size) or with the main signaling pathway of autophagy, target of rapamycin signaling (TOR). Typically, an activated TOR signaling pathway leads to the inhibition of autophagy. In our setting, down-regulation of TOR signaling might suggest activation of autophagy.

Proteins with differentially up-regulated phosphosites from Set 2 fulfilled tasks associated with the RNA processing. Processes of cellular response to heat, as well as biosynthetic and metabolic processes, were down-regulated in this set, suggesting eventual inhibition of autophagy.

String analysis suggests inhibition of autophagy through Unc-51 like autophagy activating kinase 1 (ULK1)-autophagy-related protein 13 (ATG13) pathway. STRING is a database of known and predicted protein-protein interactions. We used STRING to study the potential interactions among the proteins with differentially regulated phosphosites and to outline the functional groups of proteins identified in both sets.

In regards to Set 1 (Figure 6), we recognized two significant groups: one associated with biosynthetic and metabolic processes, and one associated with regulation of the cell cycle. In the first group, we detected proteins with up-regulated phosphosites that control lipid synthetic and metabolic processes. These proteins interact with proteins that control processes linked to energy production. The up-regulation of these proteins suggests activation of autophagy. Moreover, regulatory proteins sequestosome 1 (SQSTM1), proline-rich AKT1 substrate 1 (AKT1S1), and protein kinase AMP-activated non-catalytic subunit beta 1 (PRKAB1), which are linked with autophagy induction and formation of autophagosomes, were detected. In the second group, we detected proteins that regulate the cellular response to stress. Their up-regulation suggests activation of autophagy. Considering these findings, we assume that autophagy is activated 1 h after irradiation.

In Set 2 (Figure 7), we identified several smaller protein groups. Most of them were associated with the regulation of gene expression or transport mechanisms. The most relevant in terms of autophagy inhibition would seem to be the ULK1–ATG13 pathway. In this pathway, the mammalian target of rapamycin (mTOR) together with AMP-activated protein kinase (AMPK) play a critical role as they cooperate in phosphorylation of ULK1 at Ser638 (17). We identified ULK1 with up-regulation of a phosphosite on Ser638. There is evidence that such phosphorylation leads to reduced autophagic activity (18).

Discussion

Our previous study highlighted the benefits of combined treatment using the autophagy inhibitor, Lys05, together with IR on lung cancer cells. We demonstrated that autophagy is activated at an early stage (1 h after IR) and at a later stage (48 h after IR) is inhibited (9). However, the mechanisms regulating these processes remain unclear. In this respect, we performed a phosphoproteomic study to elucidate molecular mechanisms triggered by Lys05 treatment.

The GO analysis provided the first insight into the proteins involved in biological processes, molecular

Table I. *List of all proteins with differentially regulated phosphosites identified in Set 1.*

	Gene symbol	Protein name	Position	H/L ratio
Down-regulated	NMD3	60S ribosomal export protein NMD3	S468	−2.302
	NMD3	60S ribosomal export protein NMD3	T470	−2.302
	ERF	ETS domain-containing transcription factor ERF	T526	−1.700
	FAM193A	Protein FAM193A	S998	−1.415
	PDHA1	Pyruvate dehydrogenase E1 component subunit alpha 1	S232	−1.361
	SERBP1	Plasminogen activator inhibitor 1 RNA-binding protein	S330	−1.268
	ATP13A3	Probable cation-transporting ATPase 13A3	S540	−1.231
	ZNF462	Zinc finger protein 462	S688	−1.142
	MAP1B	Microtubule-associated protein 1B	S1852	−1.109
	MAP1B	Microtubule-associated protein 1B	S1389	−1.051
	PPIG	Peptidyl-prolyl cis-trans isomerase G	T351	−0.892
	UTP14A	U3 small nucleolar RNA-associated protein 14 homolog A	T448	−0.854
	PDHA1/2	Pyruvate dehydrogenase E1 component subunit alpha	S300	−0.850
	SRRM2	Serine/arginine repetitive matrix protein 2	S1101	−0.836
	SRRM2	Serine/arginine repetitive matrix protein 2	S1102	−0.836
	SRRM2	Serine/arginine repetitive matrix protein 2	S1103	−0.836
	PRKD2	Serine/threonine-protein kinase D2	T211	−0.835
	FARP1	FERM, RhoGEF and pleckstrin domain-containing protein 1	S427	−0.713
	AKT1S1	Proline-rich AKT1 substrate 1	T246	−0.683
	YAP1	Transcriptional coactivator YAP1	T110	−0.666
	LARP1	La ribonucleoprotein domain family member 1	S766	−0.663
Up-regulated	SLC4A7	Sodium bicarbonate cotransporter 3	S727	0.533
	SMC4	Structural maintenance of chromosomes protein 4	S41	0.535
	ARFGEF1	Brefeldin A-inhibited guanine nucleotide-exchange protein 1	S530	0.538
	ZYX	Zyxin	S312	0.605
	STMN1	Stathmin	S25	0.621
	TP53BP1	Tumor suppressor p53-binding protein 1	S530	0.640
	RSRC2	Arginine/serine-rich coiled-coil protein 2	S32	0.641
	FAM65A	Protein FAM65A	S310	0.663
	ZC3H13	Zinc finger CCCH domain-containing protein 13	S370	0.718
	ZC3H13	Zinc finger CCCH domain-containing protein 13	S372	0.718
	ZC3H13	Zinc finger CCCH domain-containing protein 13	S381	0.718
	SLC4A7	Anion exchange protein	S258	0.741
	ATN1	Atrophin-1	S77	0.755
	PRKAB1	Protein kinase AMP-activated non-catalytic subunit beta 1	S108	0.778
	RIF1	Telomere-associated protein RIF1	S2144	0.818
	SPEN	Msx2-interacting protein	S1278	0.879
	ACACA	Acetyl-CoA carboxylase alpha	S80	0.904
	SRRM2	Serine/arginine repetitive matrix protein 2	S1401	0.937
	SRRM2	Serine/arginine repetitive matrix protein 2	S1403	0.937
	SNRNP70	U1 small nuclear ribonucleoprotein 70 kDa	S410	0.945
	MPZL1	Myelin protein zero-like protein 1	Y263	0.952
	OSBPL11	Oxysterol-binding protein-related protein 11	S172	1.024
	LMNA	Prelamin-A/C;Lamin-A/C	S651	1.037
	LMNA	Prelamin-A/C;Lamin-A/C	S652	1.037
	MAP4K4	Mitogen-activated protein kinase kinase kinase kinase 4	S553	1.061
	PCYT1A	Choline-phosphate cytidylyltransferase A	S331	1.063
	PI4K2A	Phosphatidylinositol 4-kinase type 2-alpha	S462	1.076
	NUP205	Nuclear pore complex protein Nup205	S1165	1.077
	NUP98	Nuclear pore complex protein Nup98-Nup96	S1028	1.246
	SLC7A2	Cationic amino acid transporter 2	S646	1.656
	PHF12	PHD finger protein 12	S41	2.632
	AGPAT9	Glycerol-3-phosphate acyltransferase 3	S68	2.723
	KHDRBS1	KH domain-containing, RNA-binding, signal transduction-associated protein 1	S20	3.647

Table II. *List of all proteins with differentially regulated phosphosites identified in Set 2.*

|	Gene symbol	Protein name	Position	H/L ratio
Down-regulated	*PDHA1*	Pyruvate dehydrogenase E1 component subunit alpha 1	S232	−2.138
	PDHA1/2	Pyruvate dehydrogenase E1 component subunit alpha	S293	−1.881
	PDHA1/2	Pyruvate dehydrogenase E1 component subunit alpha	S300	−1.881
	FAM193A	Protein FAM193A	S998	−1.745
	SRRM2	Serine/arginine repetitive matrix protein 2	S1101	−1.372
	SRRM2	Serine/arginine repetitive matrix protein 2	S1102	−1.372
	SRRM2	Serine/arginine repetitive matrix protein 2	S1103	−1.372
	HSPB1	Heat shock protein beta-1	S15	−1.093
	ERF	ETS domain-containing transcription factor ERF	T526	−1.083
	SLAIN2	SLAIN motif-containing protein 2	S220	−1.080
	MAP4	Microtubule-associated protein 4	S1970	−0.974
	MED24	Mediator of RNA polymerase II transcription subunit 24	S38	−0.964
	MED24	Mediator of RNA polymerase II transcription subunit 24	S39	−0.964
	RRM2	Ribonucleoside-diphosphate reductase subunit M2	S20	−0.912
	SRRM2	Serine/arginine repetitive matrix protein 2	S2121	−0.895
	MKI67	Antigen KI-67	S2708	−0.845
	CLTA	Clathrin light chain A	S105	−0.832
	ATP13A3	Probable cation-transporting ATPase 13A3	S540	−0.807
	HSPB1	Heat shock protein beta-1	S82	−0.792
	LMO7	LIM domain only protein 7	S591	−0.780
	YAP1	Transcriptional coactivator YAP1	T110	−0.777
	PDHA1/2	Pyruvate dehydrogenase E1 component subunit alpha	S293	−0.739
	TPR	Nucleoprotein TPR	S2155	−0.727
	MDN1	Midasin	S4538	−0.600
	MAP4	Microtubule-associated protein 4	T538	−0.575
	PSIP1	PC4 and SFRS1-interacting protein	S106	−0.509
	MDC1	Mediator of DNA damage checkpoint protein 1	S329	−0.493
Up-regulated	*ZYX*	Zyxin	S312	0.606
	FAM65A	Protein FAM65A	S310	0.652
	NUP205	Nuclear pore complex protein Nup205	S1165	0.714
	AJUBA	LIM domain-containing protein ajuba	S119	0.716
	AHNAK	Neuroblast differentiation-associated protein AHNAK	T4766	0.732
	ZC3H13	Zinc finger CCCH domain-containing protein 13	S370	0.744
	ZC3H13	Zinc finger CCCH domain-containing protein 13	S372	0.744
	CTNND1	Catenin delta-1	S230	0.768
	KHDRBS1	KH domain-containing, RNA-binding, signal transduction-associated protein 1	S20	0.785
	CHD3	Chromodomain-helicase-DNA-binding protein 3	S1601	0.916
	CHD3	Chromodomain-helicase-DNA-binding protein 3	S1605	0.916
	SNRNP70	U1 small nuclear ribonucleoprotein 70 kDa	S410	0.919
	ITPR3	Inositol 1,4,5-trisphosphate receptor type 3	S2670	1.058
	PKP4	Plakophilin-4	S406	1.081
	UBAP2L	Ubiquitin-associated protein 2-like	S478	1.085
	DHX9	ATP-dependent RNA helicase A	S321	1.086
	RBBP6	E3 ubiquitin-protein ligase RBBP6	S1625	1.098
	ATN1	Atrophin-1	S77	1.218
	ATN1	Atrophin-1	S79	1.218
	MAP4	Microtubule-associated protein 4	S2073	1.264
	HUWE1	E3 ubiquitin-protein ligase HUWE1	S2362	1.384
	HMGXB4	HMG domain-containing protein 4	S512	1.641
	SYNGAP1	Ras/Rap GTPase-activating protein SynGAP	S423	2.706
	SYNGAP1	Ras/Rap GTPase-activating protein SynGAP	T421	2.706
	IQCA1	IQ and AAA domain-containing protein 1	S797	3.343
	GNG12	Guanine nucleotide-binding protein G(I)/G(S)/G(O) subunit gamma-12	S26	6.334
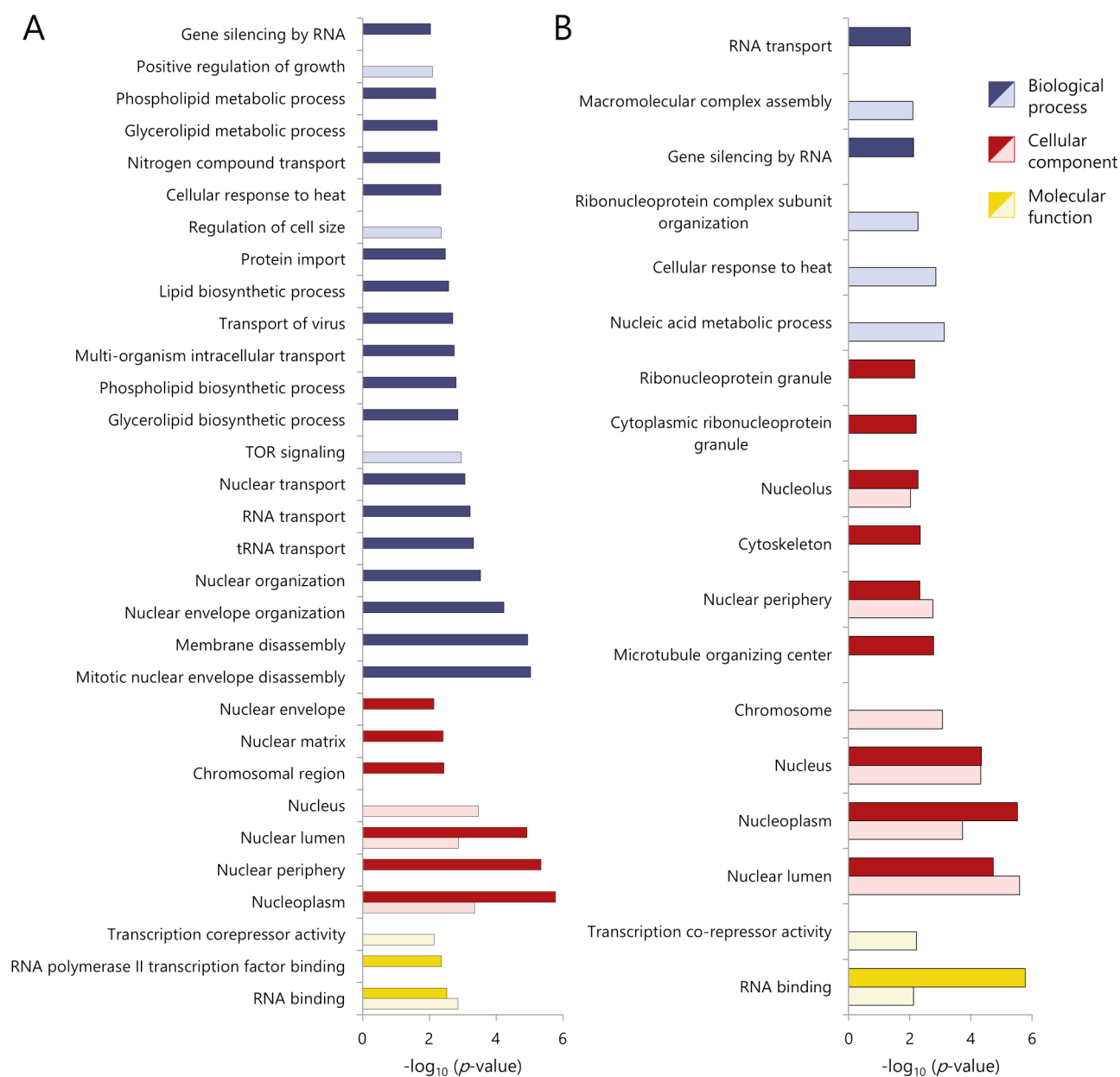
Figure 5. *Gene ontology (GO) over-representation analysis of proteins of Set 1 (A) and Set 48 2 (B) with differentially regulated phosphosites using the ConsensusPathDB level 4 terms. GO terms with darker colors correspond to proteins with up-regulated phosphosites. GO terms with brighter colors correspond to those with down-regulated phosphosites.*

functions, and cellular compartments. Analyzing data in more detail, we identified proteins with differentially regulated phosphosites that take part in autophagy.

One hour after irradiation, we identified several proteins with significantly up- or down-regulated phosphosites. Interactions between these proteins suggest the activation of autophagy early after the combined treatment by Lys05 together with IR.

We identified KH domain-containing, RNA-binding, signal transduction-associated protein 1 (KHDRBS1) as a protein with the most significantly up-regulated phosphosite 1 h after irradiation. Once phosphorylated, KHDRBS1 functions as an adapter protein in signal transduction cascades (19). It is predominantly a nuclear protein, and its primary function is to regulate alternative splicing. It influences alternative splicing of the mTOR kinase (20) and plays a role as an adapter
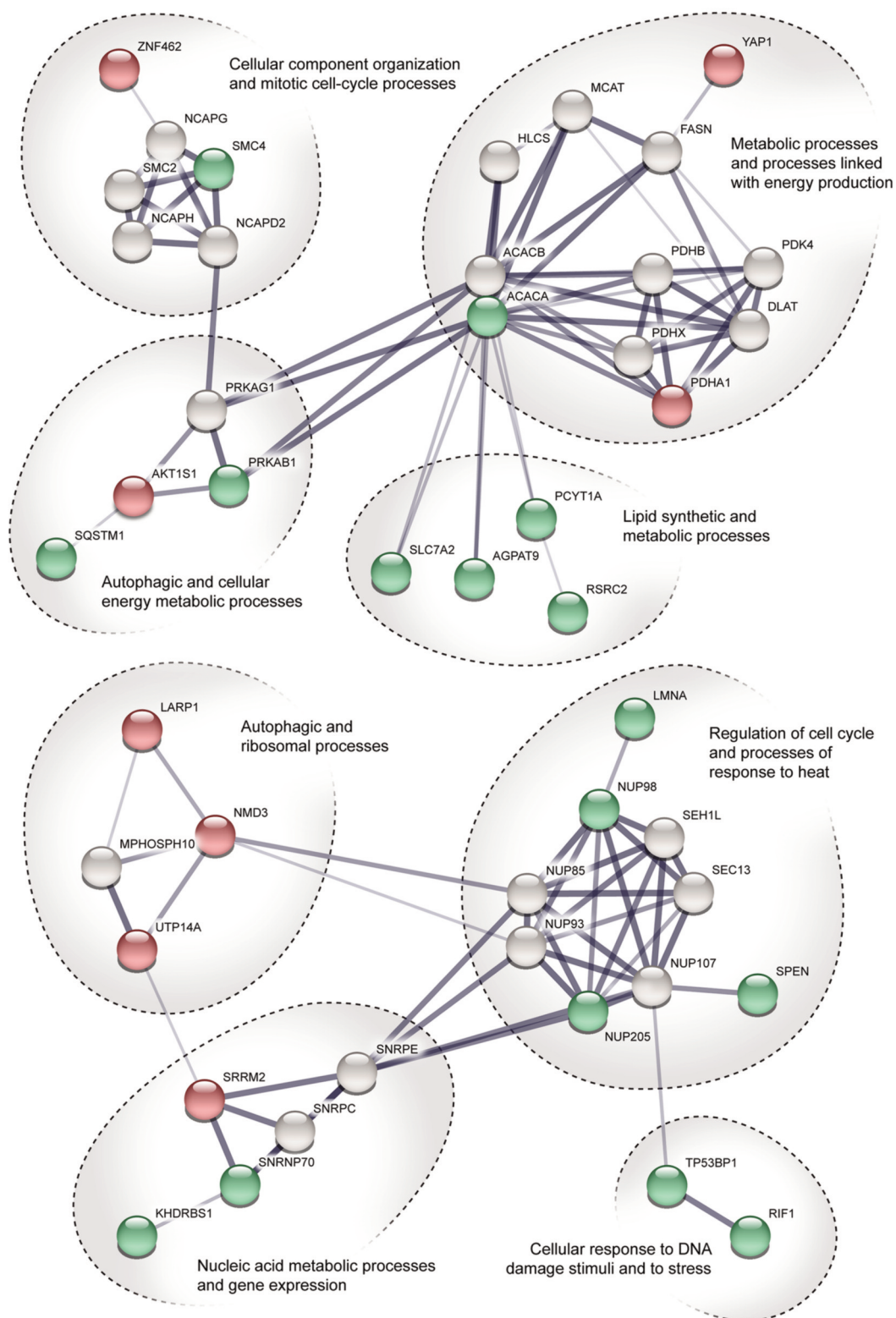
Figure 6. *STRING pathway interaction network of proteins with differentially regulated phosphosites. The figure shows the proteins identified 1 h after irradiation. Points colored green represent proteins with up-regulated phosphosites. Points colored red represent proteins with down-regulated phosphosites. Proteins colored grey were added automatically by the software. Line thickness indicates the strength of data support. See Tables I and II for protein names.*
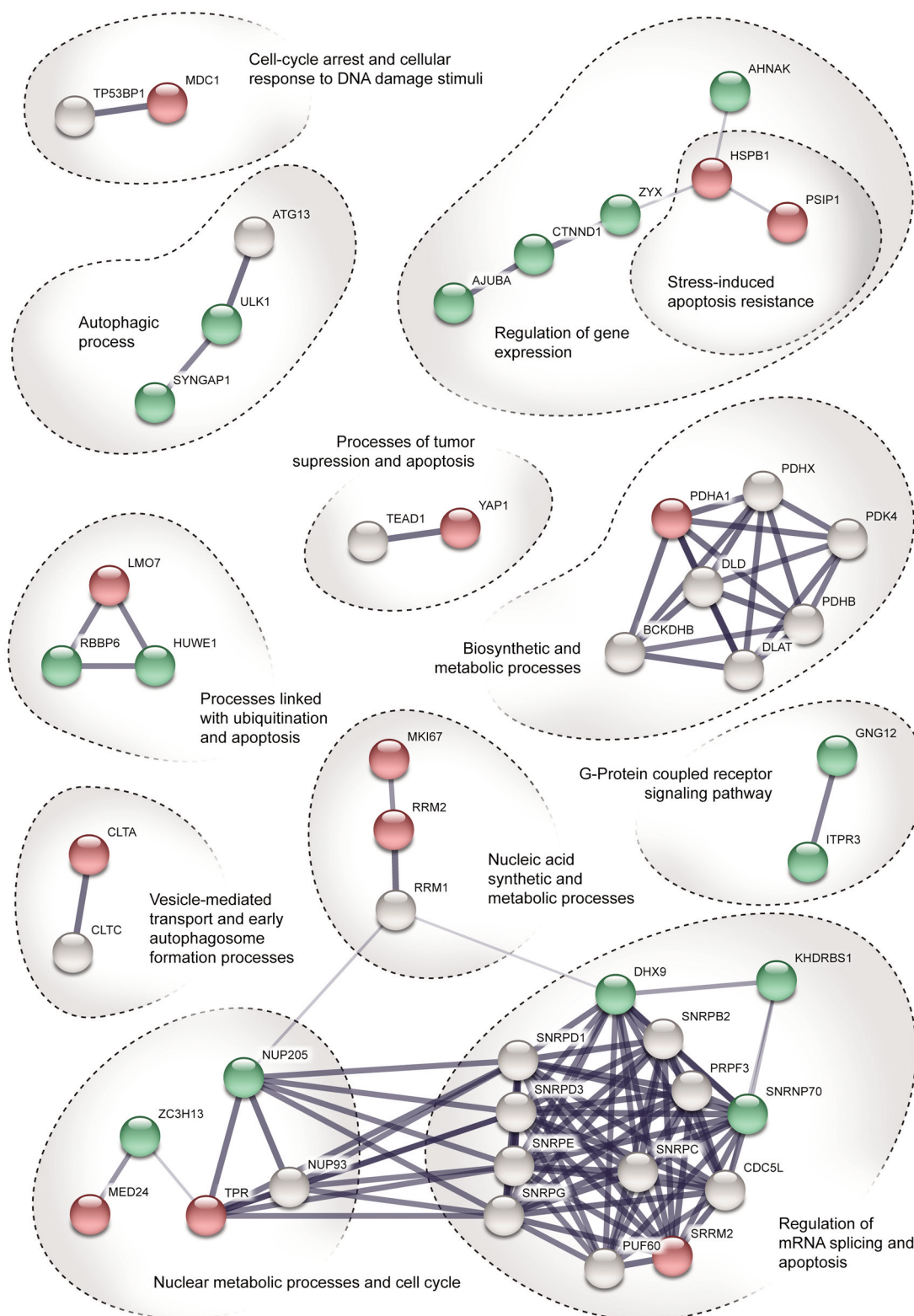
Figure 7. *STRING pathway interaction network of proteins with differentially regulated phosphosites. The figure shows the proteins identified 48 h after irradiation. Points colored green represent proteins with up-regulated phosphosites. Points colored red represent proteins with down-regulated phosphosites. Proteins colored grey were added automatically by the software. Line thickness indicates the strength of data support. See Tables I and II for protein names.*

between the autophagic machinery and misfolded proteins (21). KHDRBS1 may serve as a regulatory protein in autophagy activation since its loss in liver cells markedly attenuated liver injury caused by autophagy deficiency (22).

Furthermore, we identified glycerol-3-phosphate acyltransferase 3 (GPAT3, previously known as AGPAT9) as a protein with the second most significantly up-regulated phosphosite. GPAT3 catalyzes the initial step of de novo triacylglycerol synthesis. It transfers the acyl-group from acyl-CoA and plays a significant role in glycerolipid and phospholipid synthesis (23). It also contributes to autophagosome formation by its biosynthetic activity (24), and its function is controlled by insulin-mediated phosphorylation (25). We identified protein GPAT3 to be phosphorylated on Ser68, which is one of the 'known sites', according to PhosphoSitePlus (www.phosphositeplus.org).

SQSTM1 was another protein that was substantially up-regulated 1 h after irradiation. SQSTM1 is an autophagosome cargo protein. It targets other proteins that bind to it for selective autophagy (26). We observed this protein to be phosphorylated on Ser272. Phosphorylation of SQSTM1 on Ser272 contributes to the activation of autophagy (27).

Similarly, proteins with down-regulated phosphosites contribute to the apparent activation of autophagy early after treatment. For example, 60S ribosomal export protein NMD3 (NMD3), a protein with the most significantly down-regulated phosphosite 1 h after IR, acts as an adapter for exportin 1 (XPO1) also known as chromosomal maintenance 1 (CRM1)-mediated export of the 60S ribosomal subunit (28). According to Wengrod *et al*., inhibition of NMD3 may induce autophagy, and the hyperactivation of NMD3 may abate it (29).

AKT1S1, another protein with a down-regulated phosphosite 1 h after IR, is a subunit of mammalian target of rapamycin complex 1 (mTORC1). It possesses a regulatory function at the intersection of the AKT serine/threonine kinase 1 (AKT1) and mTORC1 signaling pathway and regulates cell growth and survival (30, 31). AKT1S1 is also an autophagy regulatory protein, which binds to regulatory associated protein of MTOR complex 1 (RAPTOR) in the mTORC1 complex. Phosphorylation of AKT1S1 by AKT causes its dissociation from RAPTOR, resulting in mTOR activation and suppression of autophagy (32). We identified AKT1S1 as having down-regulation of phosphorylation on Thr246, indicating enhanced autophagic activity. It is known that AKT can phosphorylate AKT1S1 near its C-terminus on Thr246. This phosphorylation appears to release its inhibitory effect on mTORC1 (33).

Furthermore, we identified La ribonucleoprotein domain family member 1 (LARP1), another protein tightly associated with mTOR machinery. LARP1 is a downstream substrate of mTORC1 and promotes the translation of specific classes of mRNAs. LARP1 regulates global protein synthesis, cell growth, and proliferation, as well as cell migration and invasion (34, 35). With its ability to reversibly phosphorylate and dephosphorylate, we consider LARP1 to be a phosphorylation-sensitive molecular switch in the translation of some mRNAs as well as an essential regulator of mTORC1 (36). We identified LARP1 with down-regulation of phosphosite on Ser766. This phosphosite is reportedly dephosphorylated during autophagy (37).

Taken together, all the deregulations of phosphorylated proteins mentioned above contribute to an increased rate of autophagy. The key regulators of this process appear to be the AKT1S1 pathway—initial autophagy inducer and SQSTM1 pathway—a regulator of autophagosome formation together with other regulatory proteins such as LARP1, NMD3, and GPAT3 (see Figure 6).

On the other hand, 48 h after IR, we identified proteins with significantly up- or down-regulated phosphosites that contribute to the inhibition of autophagy.

One of these proteins, Ras/Rap GTPase-activating protein SynGAP (SYNGAP1), is a Ras GTPase-activating protein that not only is critical for proper synapse function, but also takes part in other signaling processes (38). Importantly, it is a binding partner of the protein ULK1 (39), which was also detected 48 h after IR. ULK1 is a serine/threonine-protein kinase involved in autophagy regulation. It acts upstream of phosphatidylinositol 3-kinase to regulate the formation of autophagophores (the precursors of autophagosomes). ULK1 takes part in regulatory feedback loops in autophagy. It acts both as a downstream effector and a negative regulator of mTORC1 and is activated *via* phosphorylation by AMPK (40). When activated, mTORC1 inhibits autophagy by phosphorylating both ULK1 and ATG13 while reducing ULK1 kinase activity (41, 42). AMPK can also negatively regulate autophagy by phosphorylating ULK1 at Ser638, leading to reduced autophagy-related activity of ULK1 (18).

It seems that the ULK1–ATG13 pathway might be the key regulator of the late-stage inhibition of autophagy. ULK1 appears to be the crucial regulator of autophagy inhibition 48 h after irradiation (see Figure 7).

It is far beyond the extent of this article to describe in full detail all the observed alterations of phosphorylated proteins. Therefore, we outlined the most prominent ones and included an overview of all detected up- and down-regulated phosphosites in the supplementary material (Supplementary Tables I and II).

Conclusion

When performing the in-depth phosphoproteomic analysis, we expected to find autophagy somewhat inhibited early after irradiation. Instead, we found numerous deregulations of phosphorylated proteins leading to an increased rate of

autophagy. We assume that we can attribute such an effect to IR. Later after irradiation, the effect of Lys05 prevailed, as we detected phosphorylation leading to reduced autophagic activity. These findings add to the conclusions of our previous work, which confirmed inhibited autophagy by several different methodological approaches. Moreover, we presume that it is ULK1 and its binding partners which play a crucial role in such inhibition.

This work contributes to emerging phosphoproteomic insights into autophagy-mediated global signaling in lung cancer cells, which might consequently facilitate the development of precision medicine therapeutics.

Conflicts of Interest

The Authors declare that they have no conflicts of interest.

Authors' Contributions

M.O. and A.T. conceived the study and wrote the article; M.O. performed the phosphoproteomic analysis; L.C. contributed to the study design and reviewed the article; I.F. and J.K. performed mass spectrometric analysis and provided technical information; A.T. provided project administration and supervision. All Authors read and approved the article.

Acknowledgements

Funding

References

1 The American Cancer Society: Lung Cancer Statistics | How Common is Lung Cancer, 2019. Available at: https://www.cancer.org/cancer/lung-cancer/about/key-statistics.html [Last accessed on January 6, 2020]

2 Ueki N, Matsuo Y, Togashi Y, Kubo T, Shibuya K, Iizuka Y, Mizowaki T, Togashi K, Mishima M and Hiraoka M: Impact of pretreatment interstitial lung disease on radiation pneumonitis and survival after stereotactic body radiation therapy for lung cancer. J Thorac Oncol *10*: 116-125, 2015. PMID: 25376512. DOI: 10.1097/JTO.0000000000000359

3 Chaachouay H, Fehrenbacher B, Toulany M, Schaller M, Multhoff G and Rodemann HP: AMPK-independent autophagy promotes radioresistance of human tumor cells under clinical relevant hypoxia *in vitro*. Radiother Oncol *116*: 409-416, 2015. PMID: 26318663. DOI: 10.1016/j.radonc.2015.08.012

4 Dikic I and Elazar Z: Mechanism and medical implications of mammalian autophagy. Nat Rev Mol Cell Biol *19*: 349-364, 2018. PMID: 29618831. DOI: 10.1038/s41580-018-0003-4

5 Ondrej M, Cechakova L, Durisova K, Pejchal J and Tichy A: To live or let die: Unclear task of autophagy in the radio-sensitization battle. Radiother Oncol *119*: 265-275, 2016. PMID: 26993419. DOI: 10.1016/j.radonc.2016.02.028

6 Chen Y, Li X, Guo L, Wu X, He C, Zhang S, Xiao Y, Yang Y and Hao D: Combining radiation with autophagy inhibition enhances suppression of tumor growth and angiogenesis in esophageal cancer. Mol Med Rep *12*: 1645-1652, 2015. PMID: 25891159. DOI: 10.3892/mmr.2015.3623

7 Tao H, Qian P, Lu J, Guo Y, Zhu H and Wang F: Autophagy inhibition enhances radiosensitivity of ECA-109 cells *via* the mitochondrial apoptosis pathway. Int J Oncol *52*: 1853-1862, 2018. PMID: 29620258. DOI: 10.3892/ijo.2018.4349

8 Park JM, Tougeron D, Huang S, Okamoto K and Sinicrope FA: Beclin 1 and UVRAG confer protection from radiation-induced DNA damage and maintain centrosome stability in colorectal cancer cells. PloS One *9*: e100819, 2014. PMID: 24956373. DOI: 10.1371/journal.pone.0100819

9 Cechakova L, Ondrej M, Pavlik V, Jost P, Cizkova D, Bezrouk A, Pejchal J, Amaravadi RK, Winkler JD and Tichy A: A potent autophagy inhibitor (Lys05) enhances the impact of ionizing radiation on human lung cancer cells H1299. Int J Mol Sci *20*: pii: E5881, 2019. PMID: 31771188. DOI: 10.3390/ijms20235881

10 McAfee Q, Zhang Z, Samanta A, Levi SM, Ma X-H, Piao S, Lynch JP, Uehara T, Sepulveda AR, Davis LE, Winkler JD and Amaravadi RK: Autophagy inhibitor Lys05 has single-agent antitumor activity and reproduces the phenotype of a genetic autophagy deficiency. Proc Natl Acad Sci USA *109*: 8253-8258, 2012. PMID: 22566612. DOI: 10.1073/pnas.1118193109

11 Šalovská B, Fabrik I, Ďurišová K, Link M, Vávrová J, Řezáčová M and Tichý A: Radiosensitization of human leukemic HL-60 cells by ATR kinase inhibitor (VE-821): Phosphoproteomic analysis. Int J Mol Sci *15*: 12007-12026, 2014. PMID: 25003641. DOI: 10.3390/ijms150712007

12 Bendall SC, Hughes C, Stewart MH, Doble B, Bhatia M and Lajoie GA: Prevention of amino acid conversion in SILAC experiments with embryonic stem cells. Mol Cell Proteomics *7*: 1587-1597, 2008. PMID: 18487603. DOI: 10.1074/mcp.M800113-MCP200

13 Yeung Y-G and Stanley ER: Rapid detergent removal from peptide samples with ethyl acetate for mass spectrometry analysis. Curr Protoc Protein Sci *16*: Unit 16.12, 2010. PMID: 20155730. DOI: 10.1002/0471140864.ps1612s59

14 Larsen MR, Thingholm TE, Jensen ON, Roepstorff P and Jørgensen TJD: Highly selective enrichment of phosphorylated peptides from peptide mixtures using titanium dioxide microcolumns. Mol Cell Proteomics *4*: 873-886, 2005. PMID: 15858219. DOI: 10.1074/mcp.T500007-MCP200

15 Cox J and Mann M: MaxQuant enables high peptide identification rates, individualized p.p.b.-range mass accuracies and proteome-wide protein quantification. Nat Biotechnol *26*: 1367-1372, 2008. PMID: 19029910. DOI: 10.1038/nbt.1511

16 Cox J, Neuhauser N, Michalski A, Scheltema RA, Olsen JV and Mann M: Andromeda: a peptide search engine integrated into the MaxQuant environment. J Proteome Res *10*: 1794-1805, 2011. PMID: 21254760. DOI: 10.1021/pr101065j

17 Shang L and Wang X: AMPK and mTOR coordinate the regulation of ULK1 and mammalian autophagy initiation. Autophagy *7*: 924-926, 2011. PMID: 21521945. DOI: 10.4161/auto.7.8.15860

18 Puente C, Hendrickson RC and Jiang X: Nutrient-regulated phosphorylation of ATG13 inhibits starvation-induced autophagy. J Biol Chem *291*: 6026-6035, 2016. PMID: 26801615. DOI: 10.1074/jbc.M115.689646

19 KHDRBS1 - KH domain-containing, RNA-binding, signal transduction-associated protein 1 - *Homo sapiens* (Human) - *KHDRBS1* gene & protein. Available at: https://www.uniprot.org/uniprot/Q07666 [Last accessed on January 6, 2020]

20 Huot M-É, Vogel G, Zabarauskas A, Ngo CT-A, Coulombe-Huntington J, Majewski J and Richard S: The Sam68 STAR RNA-binding protein regulates mTOR alternative splicing during adipogenesis. Mol Cell *46*: 187-199, 2012. PMID: 22424772. DOI: 10.1016/j.molcel.2012.02.007

21 Chen Z, Fu Q, Shen B, Huang X, Wang K, He P, Li F, Zhang F and Shen H: Enhanced p62 expression triggers concomitant autophagy and apoptosis in a rat chronic spinal cord compression model. Mol Med Rep *9*: 2091-2096, 2014. PMID: 24715058. DOI: 10.3892/mmr.2014.2124

22 Komatsu M, Waguri S, Koike M, Sou Y-S, Ueno T, Hara T, Mizushima N, Iwata J-I, Ezaki J, Murata S, Hamazaki J, Nishito Y, Iemura S-I, Natsume T, Yanagawa T, Uwayama J, Warabi E, Yoshida H, Ishii T, Kobayashi A, Yamamoto M, Yue Z, Uchiyama Y, Kominami E and Tanaka K: Homeostatic levels of p62 control cytoplasmic inclusion body formation in autophagy-deficient mice. Cell *131*: 1149-1163, 2007. PMID: 18083104. DOI: 10.1016/j.cell.2007.10.035

23 GPAT3 - Glycerol-3-phosphate acyltransferase 3 - *Homo sapiens* (Human) - *GPAT3* gene & protein. Available at: https://www.uniprot.org/uniprot/Q53EU6 [Last accessed on January 6, 2020]

24 Dupont N, Chauhan S, Arko-Mensah J, Castillo EF, Masedunskas A, Weigert R, Robenek H, Proikas-Cezanne T and Deretic V: Neutral lipid stores and lipase PNPLA5 contribute to autophagosome biogenesis. Curr Biol CB *24*: 609-620, 2014. PMID: 24613307. DOI: 10.1016/j.cub.2014.02.008

25 Shan D, Li J, Wu L, Li D, Hurov J, Tobin JF, Gimeno RE and Cao J: GPAT3 and GPAT4 are regulated by insulin-stimulated phosphorylation and play distinct roles in adipogenesis. J Lipid Res *51*: 1971-1981, 2010. PMID: 20181984. DOI: 10.1194/jlr.M006304

26 Cassidy LD and Narita M: Cell biology. GATA get a hold on senescence. Science *349*: 1448-1449, 2015. PMID: 26404812. DOI: 10.1126/science.aad2501

27 Matsumoto G, Wada K, Okuno M, Kurosawa M and Nukina N: Serine 403 phosphorylation of p62/SQSTM1 regulates selective autophagic clearance of ubiquitinated proteins. Mol Cell *44*: 279-289, 2011. PMID: 22017874. DOI: 10.1016/j.molcel.2011.07.039

28 NMD3 - 60S ribosomal export protein NMD3 - *Homo sapiens* (Human) - *NMD3* gene & protein. Available at: https://www.uniprot.org/uniprot/Q96D46 [Last accessed on January 6, 2020]

29 Wengrod J, Martin L, Wang D, Frischmeyer-Guerrerio P, Dietz HC and Gardner LB: Inhibition of nonsense-mediated RNA decay activates autophagy. Mol Cell Biol *33*: 2128-2135, 2013. PMID: 23508110. DOI: 10.1128/MCB.00174-13

30 AKT1S1 - Proline-rich AKT1 substrate 1 - *Homo sapiens* (Human) - *AKT1S1* gene & protein. Available at: https://www.uniprot.org/uniprot/Q96B36 [Last accessed on January 6, 2020]

31 Nascimento EBM, Snel M, Guigas B, van der Zon GCM, Kriek J, Maassen JA, Jazet IM, Diamant M and Ouwens DM: Phosphorylation of PRAS40 on Thr246 by PKB/AKT facilitates efficient phosphorylation of Ser183 by mTORC1. Cell Signal *22*: 961-967, 2010. PMID: 20138985. DOI: 10.1016/j.cellsig.2010.02.002

32 Sancak Y, Thoreen CC, Peterson TR, Lindquist RA, Kang SA, Spooner E, Carr SA and Sabatini DM: PRAS40 is an insulin-regulated inhibitor of the mTORC1 protein kinase. Mol Cell *25*: 903-915, 2007. PMID: 17386266. DOI: 10.1016/j.molcel.2007.03.003

33 Yang Q and Guan K-L: Expanding mTOR signaling. Cell Res *17*: 666-681, 2007. PMID: 17680028. DOI: 10.1038/cr.2007.64

34 Tcherkezian J, Cargnello M, Romeo Y, Huttlin EL, Lavoie G, Gygi SP and Roux PP: Proteomic analysis of cap-dependent translation identifies LARP1 as a key regulator of *5'TOP* mRNA translation. Genes Dev *28*: 357-371, 2014. PMID: 24532714. DOI: 10.1101/gad.231407.113

35 Mura M, Hopkins TG, Michael T, Abd-Latip N, Weir J, Aboagye E, Mauri F, Jameson C, Sturge J, Gabra H, Bushell M, Willis AE, Curry E and Blagden SP: LARP1 post-transcriptionally regulates mTOR and contributes to cancer progression. Oncogene *34*: 5025-5036, 2015. PMID: 26921696. DOI: 10.1038/onc.2014.428. PMID: 25531318

36 Hong S, Freeberg MA, Han T, Kamath A, Yao Y, Fukuda T, Suzuki T, Kim JK and Inoki K: LARP1 functions as a molecular switch for mTORC1-mediated translation of an essential class of mRNAs. eLife *6*: e25237, 2017. PMID: 28650797. DOI: 10.7554/eLife.25237

37 Casado P, Bilanges B, Rajeeve V, Vanhaesebroeck B and Cutillas PR: Environmental stress affects the activity of metabolic and growth factor signaling networks and induces autophagy markers in MCF7 breast cancer cells. Mol Cell Proteomics *13*: 836-848, 2014. PMID: 24425749. DOI: 10.1074/mcp.M113.034751

38 SYNGAP1 - Ras/Rap GTPase-activating protein SynGAP - *Homo sapiens* (Human) - *SYNGAP1* gene & protein. Available at: https://www.uniprot.org/uniprot/Q96PV0 [Last accessed on January 6, 2020]

39 Lee JW, Park S, Takahashi Y and Wang H-G: The association of AMPK with ULK1 regulates autophagy. PloS One *5*: e15394, 2010. PMID: 21072212. DOI: 10.1371/journal.pone.0015394

40 ULK1 - Serine/threonine-protein kinase ULK1 - *Homo sapiens* (Human) - *ULK1* gene & protein. Available at: https://www.uniprot.org/uniprot/O75385 [Last accessed on January 6, 2020]

41 Alers S, Löffler AS, Wesselborg S and Stork B: The incredible ULKs. Cell Commun Signal CCS *10*: 7, 2012. PMID: 22413737. DOI: 10.1186/1478-811X-10-7

42 Lin MG and Hurley JH: Structure and function of the ULK1 complex in autophagy. Curr Opin Cell Biol *39*: 61-68, 2016. DOI: 10.1016/j.ceb.2016.02.010